Porphyrin-Incorporated 2D D–A Polymers with Over 8.5% Polymer Solar Cell Efficiency

YI-Hsiang Chao, Jyun-Fong Jheng, Jhong-Sian Wu, Kuan-Yi Wu, Hsih-Hao Peng, Ming-Chi Tsai, Chin-Li Wang, Yen-Ni Hsiao, Chien-Lung Wang, Ching-Yao Lin,* and Chain-Shu Hsu**

Significant progress in the power conversion efficiencies (PCEs) of bulk-heterojunction (BHJ) polymer solar cells (PSCs)[1] and developments in cost-effective printable plastic optoelectronics have made PSCs a promising solution to energy and environmental issues.[2] The PCE of a BHJ PSC relies on its open-circuit voltage (V_{oc}), short-circuit current (J_{sc}) and fill factor (*FF*). An efficient PSC requires both optimized molecular properties of conjugated polymers and well-controlled solid-state morphologies of the BHJ active layers made of interpenetrating polymer donor:fullerene acceptor networks. For a conjugated polymer, a suitable highest occupied molecular orbital level (E_{HOMO}) affords a high V_{oc}, an adequate lowest unoccupied molecular orbital level (E_{LUMO}) facilitates efficient charge dissociation,[3] and the intrinsic bandgap (E_g) determines its ability to harvest solar radiation. The interpenetrating network of the BHJ active layer provides maximum internal donor–acceptor interfaces for efficient charge generation and continuous *p*-type and *n*-type semiconducting channels for charge transport.[4] The molecular properties, including E_{LUMO} and E_g, together with the solid state morphology are determinative to the J_{sc} and *FF* of a PSC.

Considered as the third generation of semiconducting polymers, donor-acceptor (D–A) copolymers have been extensively explored. The wide varieties of the D and A units facilitated the adjustments of E_{HOMO}, E_{LUMO} and E_g.[3,5] However, the search of the best D–A system to achieve high PSC performance is hampered by the fact that the adjustment in the molecular structures of D and A units often causes undesired trade-off among V_{oc}, J_{sc} and *FF*. For example, although D–A polymers with low-lying E_{HOMO} would attain higher V_{oc} values,[6] the J_{sc}s could be limited by the relatively high E_gs. Narrowing E_g of a D–A polymer usually favors higher J_{sc},[7] but it could be accompanied with the elevation of E_{HOMO} and the drop of V_{oc}. Maintaining V_{oc} while decreasing E_g is also challenging because shifting E_{LUMO} downward decreases the LUMO–LUMO offset and affects the charge transfer efficiency between the polymer and the fullerene acceptors. In addition, current successes in D–A copolymers are confined within relative limited aromatic units and polymer architectures.[3] Aromatic units with more complex structures, such as porphyrins, although have unique photophysical properties, such as strong absorptions, ultrafast photoinduced charge separation and long-lived charge separation state when accompanied with fullerenes,[8] do not always improve the PCEs when incorporated into a polymer system.[9] So far, the highest PCE of porphyrin-incorporated polymer was 2.5%.[9c] Poor performances have also been observed in 2D conjugated polymers containing bulky lateral aromatic pendants.[2b,10] The rigid and large-sized lateral pendants have been suggested to complicate the physical structures, and make it challenge to obtain suitable BHJ morphology for high PCE.[9c,10]

In this study, we demonstrate a copolymerization strategy to circumvent the above-mentioned trade-offs. A common limitation in adjusting the light-harvesting ability of D–A polymers is that modifications of the D or A unit are more effective in changing E_g, but not in broadening the absorptions. Strong intramolecular charge transfer (ICT) between the D and A structural units shifts the absorption toward longer wavelength, but weakens the absorption of shorter wavelength photons. Although broadening the absorptions has the potential to increase J_{sc}, it is difficult to only fine-tune the light-harvesting ability of D–A polymers without deteriorating other properties.

We herein demonstrate that the light-harvesting ability of a D–A polymer (PTh_4FBT in **Scheme 1**)[11] can be enhanced without sacrificing its original properties and PSC performances. Through introducing a porphyrin-pyrene pendant (light harvest unit (LHU) in Scheme 1) as a complementary LHU, the copolymer (PPor-2 in Scheme 1) becomes a panchromatic absorber. The two 2,6-bis(dodecyloxy)phenyl substituents on the porphyrin moiety prevents strong aggregation of the LHU[12] as indicated from the UV–vis absorption and X-ray diffraction results. The great solubility of the LHU leads to good processability of the copolymer. Consequently, PCE of 8.0% (PCE_{avg} of 7.8%) was achieved in an additive-free process. To the best of our knowledge, this should be the highest performance in porphyrin-incorporated and 2D conjugated polymers.[2b,9,10] An even higher PCE of 8.6% was reached when 5 vol% of 1-chloronaphthalene (1-CN) was used as a processing

Y.-H. Chao, J.-F. Jheng, J.-S. Wu, K.-Y. Wu, H.-H. Peng, Prof. C.-L. Wang, Prof. C.-S. Hsu
Department of Applied Chemistry
National Chiao Tung University
1001 Ta Hsueh Road, Hsinchu 30010, Taiwan
E-mail: kclwang@nctu.edu.tw; cshsu@mail.nctu.edu.tw
M.-C. Tsai, C.-L. Wang, Y.-N. Hsiao, Prof. C.-Y. Lin
Department of Applied Chemistry
National Chi Nan University
302 University Road, Puli, Nantou 54561, Taiwan
E-mail: cyl@ncnu.edu.tw

DOI: 10.1002/adma.201401345

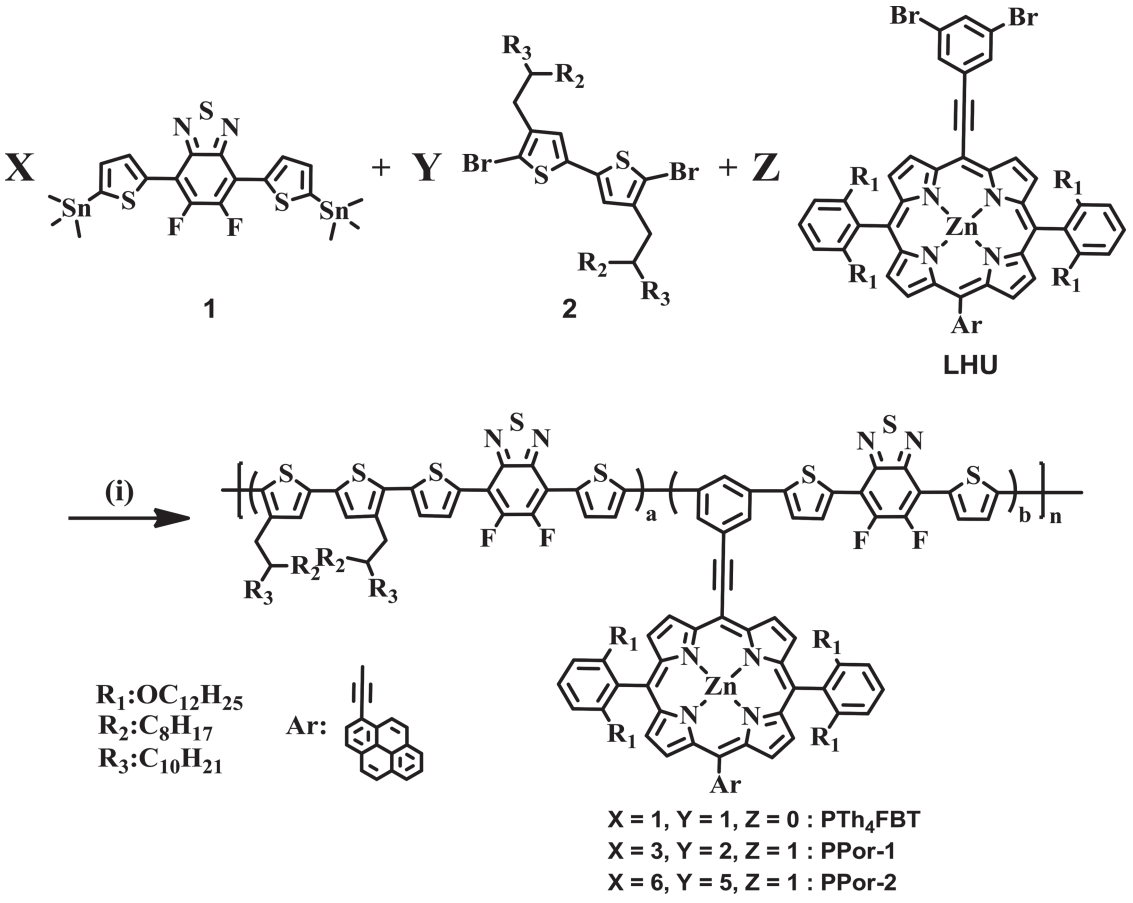

Scheme 1. Synthetic procedure of PTh_4FBT and PPors. Reagents and conditions: (i) tris(dibenzylideneacetone) dipalladium(0),tri(o-tolyl)phosphine, chlorobenzene, 180 °C, microwave 270 W, 50 min.

additive,[13] and cross-linked [6,6]-phenyl-C61-butyric styryl dendron ester (C-PCBSD) was used as a cathodic interlayer.[14]

The synthetic route of the LHU is shown in Scheme S1 in the Supporting Information.[15] The LHU exhibits typical porphyrin absorption spectra (Figure S1a, Supporting Information):[16] strong B (or Soret) bands with high extinction coefficient (ε) of 4.1×10^5 cm^{-1} M^{-1} were found in the higher-energy region, whereas weaker Q bands ($\varepsilon = 8.2 \times 10^4$ cm^{-1} M^{-1}) were observed in the lower-energy region. The film spectra in Figure S1b in the Supporting Information were obtained by air-drying pasted porphyrin solutions on glass. The film absorption bands are red-shifted from those in solution, which suggests J-type aggregation of the LHU.[17]

To verify the influences and the optimized ratio of the LHU, two PPors (PPor-1 and PPor-2) were prepared via microwave-assisted Stille-coupling copolymerization among 5,6-difluoro-4,7-bis[5-(trimethylstannyl) thiophen-2-yl]benzo-2,1,3-thiadiazole (**1**), 5,5′-dibromo-4,4′-bis(2-octyldodecyl)-2,2′-bithiophene (**2**), and LHU (Scheme 1). The molar ratio of **1**:**2**:LHU = 3:2:1 was used to prepare PPor-1, and the ratio of **1**:**2**:LHU = 6:5:1 was used to prepared PPor-2. The PPors were obtained as black solids. Compared with PTh_4FBT, the solubility of the PPors are improved likely because the presence of the LHUs. These solids are readily soluble in tetrahydrofuran (THF) and chlorinated solvents. The molecular weight of PPor-1 and PPor-2 were 29.9 kDa (PDI = 1.62) and 38.9 kDa (PDI = 1.82), respectively, as determined by gel-permeation chromatography (GPC). Both PPors show 5% weight loss temperatures above 440 °C as determined from the thermogravimetric analysis shown in Figure S2 in the Supporting Information.

The thin-film UV–vis absorption spectra of PPors along with PTh_4FBT are shown in **Figure 1**. The B band absorptions of the incorporated LHUs were observed in the PPors. Higher LHU feed ratio in PPor-1 (16 mol%) resulted in a stronger B band absorption, but a weaker ICT band absorption, while the lower LHU feed ratio (8.3 mol%) of PPor-2 led to nearly identical B band and ICT band intensities, thus gave a panchromatic light absorber with more balanced absorption across the entire visible-light region. It is noteworthy to mention that λ_{max} of the B bands (466 nm) in the PPor thin films are identical to that of the LHU in dilute solution (Figure S1a, Supporting Information), strongly suggesting that the porphyrin units should be dispersed instead of aggregated in the PPor thin films. On the other hand, the shoulder band located at λ_{max} of 690 nm is related to aggregation of the conjugated backbones as in the case of PTh_4FBT.[11] Thus, the weaker 690 nm absorption shoulder of the PPors implies that the presence of the bulky LHUs weakens the intermolecular interaction among the polymer backbones, consistent with the better solubility of the PPors. The E_gs of PPor-1 and PPor-2 are 1.65 eV

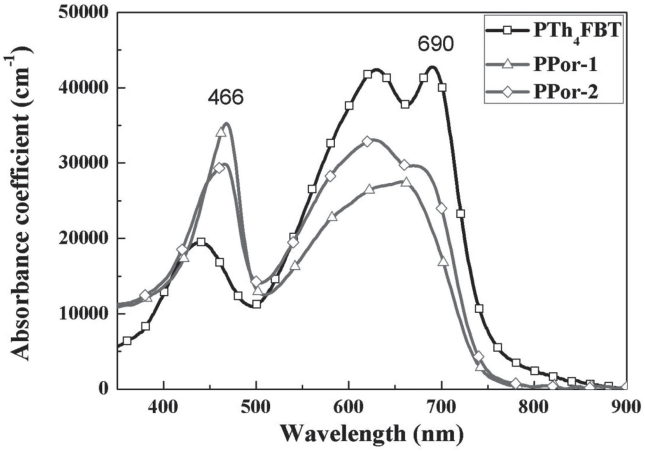

Figure 1. UV–vis absorption spectra of PTh$_4$FBT and PPors thin films.

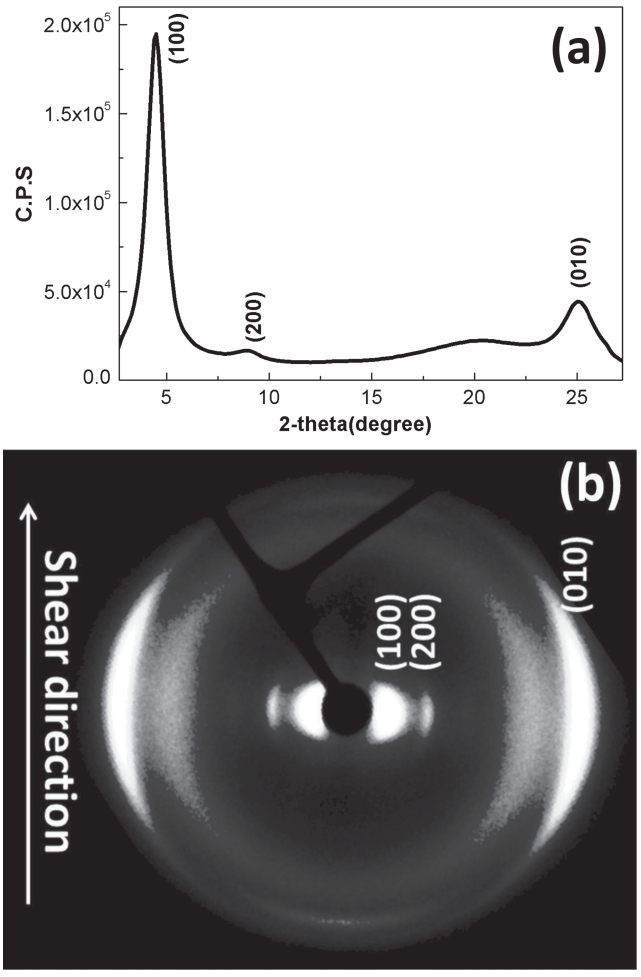

Figure 2. a) 1D Powder XRD of PPor-2 and b) 2D fiber XRD pattern of the sheared PPor-2. The solid arrow indicates the direction of mechanical shearing force applied on the sample.

and 1.63 eV, respectively, deduced from the thin film absorption edge. Figure S3 in the Supporting Information shows the cyclic voltammetry (CV) of the PPors. The E_{HOMO} is −5.29 eV for PPor-1 and −5.30 eV for PPor-2. The E_{LUMO} of both PPors is −3.31 eV. The energy levels were determined based on their onset redox potentials. Compared to PTh$_4$FBT,[11] the inclusion of the LHU units elevated the E_{HOMO}s and E_{LUMO}s of the conjugated polymers.

The influences of the porphyrin LHU to the phase behavior and phase structures were studied by differential scanning calorimetry (DSC) and X-ray diffraction (XRD). In the DSC analysis (Figure S4, Supporting Information), only broad transition humps around 260 °C were observed for PPor-1. On the contrary, an endothermic transition at 264 °C (ΔH = 3.05 J g^{-1}) and an exothermic transition at 245 °C (ΔH = 3.08 J g^{-1}) were clearly observed for PPor-2. The results suggested that solid-state structure of PPor-1 is close to amorphous, but PPor-2 is in an ordered phase below 264 °C. However, the transition heat and temperature of PPor-2 are lower than those of PTh$_4$FBT,[11] indicating that the presence of the bulky LHUs decreases the stability and order of the solid-state structure. The ordered structure of PPor-2 was characterized by 1D powder XRD and 2D fiber XRD patterns of PPor-2. Diffraction peaks located at 2θ = 4.27°, 8.57°, and 25.1° were observed in the 1D XRD pattern (**Figure 2**a). In the 2D fiber pattern (Figure 2b), these three diffraction peaks were identified along the equator (perpendicular to the shear direction), and suggests that the normal directions of the periodic structures are perpendicular to the chain axis. The two diffraction peaks at low-angle region have a scattering factor (q) ratio of 1:2, and can be indexed as (100) and (200) diffraction peaks of an ordered lamellar structure with d-spacing of 2.07 nm. The rest one at 25.1° is attributed to the ordered π–π stacking with d-spacing of 0.36 nm. Notably, the diffraction pattern of PPor-2 resembles that of PTh$_4$FBT.[11] This implies that conjugated backbones are packed ordered in the solid state, but the order arrangement of the LHU pendants is absent. Although the backbones are still packed orderly, the presence of the LHUs did decrease the solid-state order. The correlation lengths of the lamellar structure (L_{100}) and π–π stacking (L_{010}) of PPor-2 are 7.8 nm and 5.6 nm, respectively. They are shorter than the L_{100} (38.8 nm) and L_{010} (6.0 nm) of PTh$_4$FBT. Thus, the bulky lateral LHU degraded the order of the periodic structures, and the influence is more pronounced to the lamellar structure than to the π–π stacking. The significant decrease in the L_{100} of PPor-2 could be an indication that the LHUs are dispersed with the lateral 2-octyldodecyl chains in the lamellar structure. It is speculated that the presence of the rigid and bulky porphyrin LHU disrupted the segregation between the conjugated backbone and the flexible 2-octyldodecyl side chains, and decreased the L_{100} of the lamellar structure. PPor-2 is one of the very scarce cases to keep the ordered packing of the conjugated backbone in the 2D conjugated polymers, which possess various rigid and bulky lateral groups.[2b,9c,10]

The hole mobility (μ_h) of PPor-2 was studied in organic field-effect transistor (OFET) devices. The results were summarized in Table S1 in the Supporting Information. The output and transfer plots of PPor-2 (Figure S5, Supporting Information) exhibited typical p-channel OFET characteristics. Highest μ_h of 5.72 × 10^{-2} cm^2 V^{-1} s^{-1} was delivered after annealing PPor-2 at 250 °C. The highest μ_h of PPor-2 is lower than that of PTh$_4$FBT (0.29 cm^2 V^{-1} s^{-1}). Therefore, the presence of bulky LHU also deteriorated the charge mobility of

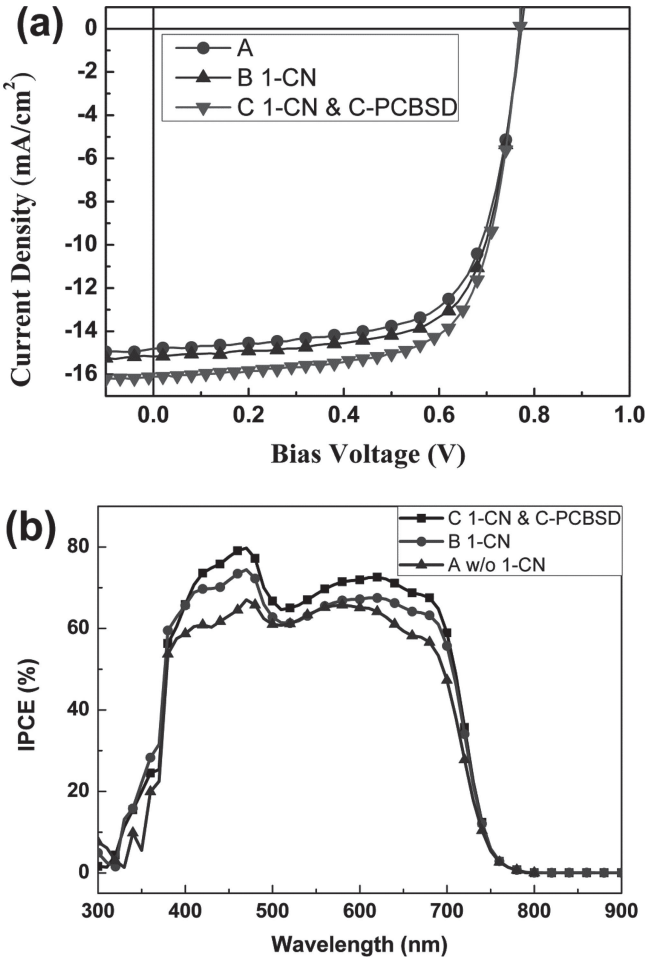

Figure 3. a) *J–V* characteristics and b) IPCE spectra of PPor-2:$PC_{71}BM$-based inverted BHJ PSCs under illumination of AM 1.5 G at 100 mW cm^{-2}.

the D–A polymer. The photovoltaic performance of PPor-2 was first evaluated in inverted BHJ PSCs with architecture of indium tin oxide (ITO)/ZnO (40 nm)/PPor-2:$PC_{71}BM$ (1:2, w/w)/MoO_3 (7 nm)/Ag (150 nm). The device is denoted as Device A. The *J–V* characteristics of Device A are shown in **Figure 3**a and summarized in **Table 1**. PPor-2:$PC_{71}BM$ devices delivered a PCE up to 8.0% (PCE_{avg} of 7.8%) with a V_{oc} of 0.78 V, a J_{sc} of 14.9 mA cm^{-2}, and an *FF* of 67%. Compared with the PTh_4FBT:$PC_{71}BM$ PSCs[11] (Table 1), PPor-2 gave a better J_{sc} while keeping a nearly identical V_{oc} and *FF*. Consequently, a higher PCE was achieved in the PPor-2 PSCs. The result represents a successful case to circumvent the common V_{oc}–J_{sc} trade-off via incorporating proper amount of LHUs into a well-performed D–A polymer, and verifies the usefulness of the copolymerization strategy.

Table 1. Characteristic properties of the PPor-2:$PC_{71}BM$ PSCs.

Device	Polymer	V_{oc} [V]	J_{sc} [mA cm^{-2}]	*FF* [%]	PCE_{max} (PCE_{ave})[a)] [%]
Ref.	PTh_4FBT	0.77	13.5	66	6.8 (6.7)
A	PPor-2	0.78	14.9	67	8.0 (7.8)
B	PPor-2[b)]	0.77	15.2	68	8.2 (8.0)
C	PPor-2[c)]	0.77	16.1	70	8.6 (8.4)

A higher PCE of 8.2% (PCE_{avg} of 8.0%) was reached in Device B, where 5 vol% of 1-chloronaphthalene (1-CN) were used as a processing additive. As shown in Figure 3a and Table 1, the higher PCE is a result of the improved J_{sc} and *FF*. In the incident-photon to current conversion efficiency (IPCE) curve of Device B (Figure 3b), over 60% of IPCE was observed from 400 to 700 nm, explaining the high J_{sc}. Notably, an additional hump from 400 to 500 nm, which is absent in the IPCE curve of the PTh_4FBT:$PC_{71}BM$ devices, [11] reached over 70% IPCE. This hump correlates with the B-band absorption of the LHUs in PPor-2, which confirms the efficacy of the porphyrin LHU as a complementary unit to compensate the low absorbance of the conjugated backbone in the blue-light region.

A superior PCE of 8.6% (PCE_{avg} of 8.4%) was achieved in Device C where C-PCBSD was adopted as a cathodic interlayer. The presence of the C-PCBSD interlayer elevated the overall IPCE of the PPor-2:$PC_{71}BM$ devices (Figure 3b), and thus the J_{sc} further increased to 16.1 mA cm^{-2}. In the dark, Device C showed a reduced current density at reversed biases and a better diode rectification ratio (Figure S6, Supporting Information). The improved J_{sc} and *FF* of Device C can be attributed to the improved exciton dissociation and diminished leakage pathways due to the presence of C-PCBSD interlayer.[14] Thus, the simultaneous increases in J_{sc} and *FF* led to the best performance even reported for the porphyrin-incorporated and 2D conjugated polymers.

In summary, a copolymerization strategy was developed to incorporate prophyrin LHU into a D–A polymer. Proper amount of LHU made the PPor a panchromatic light absorber. The additive-free PPor-2:$PC_{71}BM$ devices delivered PCE up to 8.0%, and represented a breakthrough in porphyrin-incorporated and 2D conjugated copolymers. An even higher PCE of 8.6% was reached when a C-PCBSD cathodic interlayer were placed to diminish leakage current. Compared to the PTh_4FBT:$PC_{71}BM$ counterparts, the *J–V* characteristics and IPCE curves of the PPor-2:$PC_{71}BM$ devices clearly showed the improvements in J_{sc} and *FF*. The copolymerization strategy thus provides flexibility in fine-tuning the well-performed copolymers and circumventing the common V_{oc}–J_{sc} trade-off. It also represents an approach to leverage unique properties of complicated lateral aromatic pendants.

Experimental Section

General Measurements and Characterization: ^{1}H-NMR was carried out by using a Bruker Avance II 300 MHz NMR Spectrometer. Gel-permeation chromatography (GPC) was measured using a Viscotek GPC system equipped with a Viscotek T50A differential viscometer, and Viscotek LR125 laser refractometer. Three 10 cm American Polymer columns were connected in series in the order of decreasing pore size (10^5, 10^4, and 10^3 Å); polystyrene standards were used for calibration, and tetrahydrofuran (THF) was used as the eluent. Differential scanning calorimetry (DSC) was performed on a TA Q200 Series DSC and operated at a scan rate of 10 °C min^{-1}. Thermogravimetric analysis (TGA) was carried out using a Perkin–Elmer Pyris 7 instrument at a scan rate of 10 °C min^{-1}. UV–vis spectra were measured using an HP 8453 spectrophotometer. The cyclic voltammograms (CV) were conducted on a Bioanalytical System analyzer with a standard three-electrode cell (a glassy carbon working electrode, a

Pt auxiliary electrode, and a Ag/AgCl reference electrode) in acetonitrile solutions containing 0.1 M tetrabutylammonium hexafluorophosphate as the electrolyte. The CV curves were calibrated using ferrocene as the internal standard, whose oxidation potential is set at –4.8 eV with respect to zero vacuum level. For XRD patterns, a Bruker apex duo single crystal diffraction instrument was used and a INCOATEC 18 kW rotating I microfocus X-ray generator(Cu Kα radiation (0.1542 nm)) attached to an APEX II CCD camera was used. The exposure time to obtain high-quality patterns was 40 s.

OFET Device Fabrication and Characterization: An n-type heavily doped Si wafer with a SiO_2 layer of 300 nm and a capacitance of 11 nF cm^{-2} was used as the gate electrode and dielectric layer. Thin films (40–60 nm in thickness) of polymers were deposited on octadecyltrichlorosilane (ODTS)-treated SiO_2/Si substrates by spin-coating their *o*-dichlorobenzne (DCB) solution (5 mg mL^{-1}). The thin films were annealed at 200 °C for 10 min. Gold source and drain contacts (40 nm in thickness) were deposited by vacuum evaporation on the organic layer through a shadow mask, affording a bottom-gate, top-contact OFET device. Electrical measurements of the OFET devices were carried out at room temperature in air using a 4156C Semiconductor Parameter Analyzers, Agilent Technologies. The field-effect mobility was calculated in the saturation regime by using the equation, $I_{ds} = (\mu WC_i/2L)(V_g - V_t)^2$, where I_{ds} is the drain-source current, μ is the field-effect mobility, W is the channel width (1 mm), L is the channel length (0.1 mm), C_i is the capacitance per unit area of the gate dielectric layer, V_g is the gate voltage, and V_t is threshold voltage.

BHJ PSC Fabrication and Characterization: The device structures were ITO/ZnO/polymer:$PC_{71}BM$/MoO_3/Ag for Device A and Device B; and ITO/ZnO/C-PCBSD/polymer:$PC_{71}BM$/MoO_3/Ag for Device C. The optimized thickness was 110 nm for the PPor-2:$PC_{71}BM$ active layer, and 96 nm for the PTh_4FBT:$PC_{71}BM$ active layer. The ITO glass substrates were cleaned with detergent, deionized water, acetone, and isopropyl alcohol in an ultrasonic bath and then dried overnight in an oven at >100 °C. Zinc acetate dihydrate (Aldrich) dissolved in 2-metoxyenthanol (10 mg mL^{-1}) and small amount of ethanolamine was spin-cast on pre-cleaned ITO substrates and baked at 180 °C for 10 minutes in the air to form the ZnO layer with thickness of 40 nm. [6,6]-Phenyl-C61-butyric styryl dendron ester (PCBSD) was dissolved in *o*-dichlorobenzene (ODCB) to a concentration of 0.5 wt%. For devices fabricated with C-PCBSD interlayer, the PCBSD solution was spin-cast onto the ZnO layer to form a thin film with a thickness of ca. 10 nm. Subsequently, the film was annealed at 180 °C for 10 min in the glove box for thermal cross-linking. For Device A, PPor-2 was dissolved in ODCB (0.77 wt%), and $PC_{71}BM$ was then added into the solution to reach the desired weight ratio. For Device B and C, 5 vol% of 1-chloronaphtholene (1-CN) was also added into the solution. The solution was stirred at 70 °C for overnight and filtrated through a 0.45 μm filter. The active layers were then spin-coated onto the ZnO layer at 900 rpm. The anode made of MoO_3 (6 nm) and Ag (150 nm) was evaporated through a shadow mask under vacuum (<10^{-6} Torr). Each sample consists of four independent pixels defined by an active area of 0.04 cm^2. The devices were encapsulated and characterized in air under 100 mW cm^{-2} AM 1.5 simulated light measurement (Yamashita Denso solar simulator). Current–voltage (*J*–*V*) characteristics of the PSCs were obtained using a Keithley 2400 SMU. Solar illumination conforming the JIS Class AAA was provided by a SAN-EI 300W solar simulator equipped with an AM 1.5G filter. The light intensity was calibrated with a Hamamatsu S1336–5BK silicon photodiode.

Materials: All the chemicals were purchased from Aldrich, Lancaster, TCI, or Acros, and were used as received unless otherwise specified. 5,6-difluoro-4,7-diiodobenzo-2,1,3-thiadiazole (**1**), 5,5′-dibromo-4,4′-bis(2-octyldodecyl)-2,2′-bithiophene (**2**), and porphyrin-pyrene LHU were synthesized according to the literature.[1] Phenyl-C_{71}-butyric acid methyl ester ($PC_{71}BM$) was purchased from Nano-c. The monomers was synthesized according to Scheme S1 in the Supporting Information, and the polymers were synthesized according to Scheme 1.

Synthesis: The synthesis of the porphyrin is similar to that in our past reports.[11,12,18] As shown in Scheme S1 in the Supporting Information, the procedures involve reacting brominated porphyrins with suitable substituents according to Sonogashira cross-coupling methods.[19]

LHU: 316 mg of dibrominated porphyrin **4** (m.w. = 1420.98 g mol^{-1}, 0.22 mmol.) were dissolved in 35 mL of dried THF, and 5 mL of dried Et_3N and 0.9 eq. pyrene-acetylene were added. The solutions were then degassed by 3 cycles of the freeze–pump–thaw technique, followed adding 15 mol% of $Pd(PPh_3)_4$ and CuI under an inert atmosphere in a glovebox. The reaction was then stirred at 40 °C for 20 h. The completion of the reaction was monitored by TLC. Upon completion, the reaction solution was evaporated under reduced pressure. The residue was then re-dissolved in CH_2Cl_2, followed by $NH_4Cl_{(aq)}$ washes, then dried over Na_2SO_4. After chromatographic separation on silica gel with THF/hexanes (1/10) and crystallization from CH_2Cl_2/MeOH, porphyrin **5** was collected as dark green solids at 30% yield. 142 mg of the mono-brominated porphyrin **5** (m.w. = 1566.34 g mol^{-1}, 0.09 mmol.) was dissolved in 35 mL of dried THF, and 5 mL of dried Et_3N and 10 eq. of triisopropylsilylacetylene (TIPS-acetylene) were added. The solutions were then degassed by 3 cycles of the freeze–pump–thaw technique, followed by adding 20 mol% of $Pd(PPh_3)_2Cl_2$ and CuI under an inert atmosphere in a glovebox. The reaction was then stirred at 60 °C for 6 h. The completion of the reaction was monitored by TLC. Upon completion, the reaction solution was evaporated under reduced pressure. The residue was then re-dissolved in CH_2Cl_2, washed with $NH_4Cl_{(aq)}$ solutions, then dried over Na_2SO_4. After chromatographic separation on silica gel with THF/hexanes (1/10) and crystallization from CH_2Cl_2/MeOH, porphyrin **6** was collected as dark green solids at 98% yield. For the deprotection of the TIPS group, porphyrin **6** was first dissolved in dried THF, followed by the addition of 1 eq. of tetrabutylammonium fluoride (1M in THF) and stirring at 0 °C in the dark for 1 h. The completion of the reaction was monitored by TLC. Upon completion, the reaction solution was evaporated under reduced pressure. The residue was then redissolved in CH_2Cl_2, washed with $NH_4Cl_{(aq)}$ solutions, and dried over Na_2SO_4. After evaporation under reduced pressure, porphyrin **7** was used immediately to react with 50 eq. of tribromobenzene to afford 70% of LHU as dark green solids after chromatographic separation on silica gel with THF/hexanes (1/10), followed by crystallization from CH_2Cl_2/MeOH.

^{1}H-NMR ($CDCl_3$ at 7.26 ppm, 300 MHz, δ): 9.93(d, J = 4.6Hz, 2H), 9.59(d, J = 4.2Hz, 2H), 9.30(d, J = 9.0Hz, 1H), 8.96(d, J = 4.6Hz, 2H), 8.90(d, J = 4.5Hz, 2H), 8.70(d, J = 8.0Hz, 1H), 8.42–8.22(overlapped, 4H), 8.17(s, 2H), 8.15–8.00(overlapped, 3H), 7.80–7.67(overlapped, 3H), 7.03(d, J = 8.4Hz, 4H), 3.88(t, J = 6.3Hz, 8H), 1.62–1.50(m, overlapped, 38H), 1.22–0.70(m, overlapped 46H), 0.70–0.32(m, overlapped, 24H). Elemental Analysis: $C_{106}H_{126}Br_2N_4O_4Zn$, Calcd. C 72.94%, H 7.28%, N 3.21%; found C 72.93%, H 7.49%, N 2.89%. Mass (M^+) Calcd. 1740.74, found 1740.92.

PPor-1:5,5′-Dibromo-4,4′-bis(2-octyldodecyl)-2,2′-bithiophene (60.7 mg, 0.07 mmol), 5,6-difluoro-4,7-bis[5-(trimethylstannyl)thiophen-2-yl]benzo-2,1,3-thiadiazole (68.1 mg, 0.103 mmol), LHU (59.9 mg, 0.034 mmol), tris(dibenzylideneacetone) dipalladium (4.7 mg, 0.005 mmol), tri(2-methylphenyl)phosphine (12.5 mg, 0.04 mmol) and deoxygenated chlorobenzene (5 mL) were added to a 50 mL round bottom flask. The mixture was then degassed by bubbling nitrogen for 10 min at room temperature. The round-bottom flask was put into a microwave reactor and heated to 180 °C under 270 W for 50 min. Then, tributyl(thiophen-2-yl)stannane (10.5 mg, 0.028 mmol) was added to the mixture solution and reacted for 10 minutes under 270 W. Finally, 2-bromothiophene (20 mg, 0.123 mmol) was added to the mixture solution and reacted for 10 min under 270 W. After cooling to room temperature, the solution was added dropwise to methanol. The precipitate was collected by filtration and washed by Soxhlet extraction with acetone (24 h) and hexane (24 h) sequentially. The residue solid was redissolved in hot THF (100 mL). The Pd-thiol gel (Silicycle Inc.) was added to above THF solution to remove the residual Pd catalyst at 70 °C for 12 h. After filtration of solution and removal of the solvent under reduced pressure, the polymer solution was added into methanol to reprecipitate it. The purified polymer was collected by filtration and dried under vacuum for 1 day to give a black solid. Yield: 100 mg (72.2%). M_n = 29.9 kDa; PDI = 1.62.

PPor-2: 5,5′-Dibromo-4,4′-bis(2-octyldodecyl)-2,2′-bithiophene (85.5 mg, 0.097 mmol), 5,6-difluoro-4,7-bis(5-(trimethylstannyl)thiophen-2-yl) benzo-2,1,3-thiadiazole (76.7 mg, 0.116 mmol), LHU (33.7 mg, 0.019 mmol), tris(dibenzylideneacetone) dipalladium (5.3 mg, 0.006 mmol), tri(2-methylphenyl)phosphine (14.1 mg, 0.05 mmol) and deoxygenated chlorobenzene (5 mL) were added to a 50 mL round bottom flask. The mixture was then degassed by bubbling nitrogen for 10 min at room temperature. The round-bottom flask was put into a microwave reactor and heated to 180 °C under 270 W for 50 min. Then, tributyl(thiophen-2-yl)stannane (10.5 mg, 0.028 mmol) was added to the mixture solution and reacted for 10 min under 270 W. Finally, 2-bromothiophene (20 mg, 0.123 mmol) was added to the mixture solution and reacted for 10 min under 270 W. After cooling to room temperature the solution was added dropwise to methanol. The precipitate was collected by filtration and washed by Soxhlet extraction with acetone (24 h) and hexane (24 h) sequentially. The residue solid was re-dissolved in hot THF (100 mL). The Pd-thiol gel (Silicycle Inc.) was added to the above THF solution to remove the residual Pd catalyst at 70 °C for 12 h. After filtration of the solution and removal of the solvent under reduced pressure, the polymer solution was added into methanol to reprecipitate it. The purified polymer was collected by filtration and dried under vacuum for 1 day to give a black purple solid. Yield: 95 mg (68.1%). M_n = 38.9 kDa; PDI = 1.82.

Supporting Information

Supporting Information is available from the Wiley Online Library or from the author.

Acknowledgements

This work was supported by the National Science Council and "ATP" of the National Chiao Tung University and Ministry of Education, Taiwan.

Received: March 26, 2014
Revised: May 6, 2014
Published online: June 2, 2014

[1] a) J. B. You, L. T. Dou, K. Yoshimura, T. Kato, K. Ohya, T. Moriarty, K. Emery, C. C. Chen, J. Gao, G. Li, Y. Yang, *Nat. Commun.* **2013**, *4*, 1446; b) I. Osaka, T. Kakara, N. Takemura, T. Koganezawa, K. Takimiya, *J. Am. Chem. Soc.* **2013**, *135*, 8834; c) K. H. Hendriks, G. H. L. Heintges, V. S. Gevaerts, M. M. Wienk, R. A. J. Janssen, *Angew. Chem. Int. Ed.* **2013**, *52*, 8341; d) Z. C. He, C. M. Zhong, S. J. Su, M. Xu, H. B. Wu, Y. Cao, *Nat. Photonics* **2012**, *6*, 591; e) S. J. Liu, K. Zhang, J. M. Lu, J. Zhang, H. L. Yip, F. Huang, Y. Cao, *J. Am. Chem. Soc.* **2013**, *135*, 15326; f) H. X. Zhou, L. Q. Yang, A. C. Stuart, S. C. Price, S. B. Liu, W. You, *Angew. Chem. Int. Ed.* **2011**, *50*, 2995; g) C. M. Amb, S. Chen, K. R. Graham, J. Subbiah, C. E. Small, F. So, J. R. Reynolds, *J. Am. Chem. Soc.* **2011**, *133*, 10062; h) Y. H. Chao, J. S. Wu, C. E. Wu, J. F. Jheng, C. L. Wang, C. S. Hsu, *Adv. Energy Mater.* **2013**, *3*, 1279; i) X. G. Guo, N. J. Zhou, S. J. Lou, J. Smith, D. B. Tice, J. W. Hennek, R. P. Ortiz, J. T. L. Navarrete, S. Y. Li, J. Strzalka, L. X. Chen, R. P. H. Chang, A. Facchetti, T. J. Marks, *Nat. Photonics* **2013**, *7*, 825.

[2] a) A. J. Heeger, *Chem. Soc. Rev.* **2010**, *39*, 2354; b) Y. F. Li, *Acc. Chem. Res.* **2012**, *45*, 723.

[3] a) M. C. Scharber, D. Wuhlbacher, M. Koppe, P. Denk, C. Waldauf, A. J. Heeger, C. L. Brabec, *Adv. Mater.* **2006**, *18*, 789; b) H. L. Yip, A. K. Y. Jen, *Energy Environ. Sci.* **2012**, *5*, 5994; c) J. Peet, A. J. Heeger, G. C. Bazan, Acc. Chem. Res.*zan, Acc. Chem. Res.* **2009**, *42*, 1700.

[4] a) G. Yu, J. Gao, J. C. Hummelen, F. Wudl, A. J. Heeger, *Science* **1995**, *270*, 1789; b) S. J. Lou, J. M. Szarko, T. Xu, L. P. Yu, T. J. Marks, L. X. Chen, *J. Am. Chem. Soc.* **2011**, *133*, 20661.

[5] a) Y. J. Cheng, S. H. Yang, C. S. Hsu, *Chem. Rev.* **2009**, *109*, 5868; b) A. Facchetti, *Chem. Mater.* **2011**, *23*, 733; c) H. X. Zhou, L. Q. Yang, W. You, *Macromolecules* **2012**, *45*, 607; d) F. He, L. P. Yu, *J. Phys. Chem. Lett.* **2011**, *2*, 3102.

[6] a) M. S. Su, C. Y. Kuo, M. C. Yuan, U. S. Jeng, C. J. Su, K. H. Wei, *Adv. Mater.* **2011**, *23*, 3315; b) G. Zhang, Y. Fu, Z. Xie, Q. Zhang, *Macromolecules* **2011**, *44*, 1414; c) C. Piliego, T. W. Holcombe, J. D. Douglas, C. H. Woo, P. M. Beaujuge, J. M. J. Fréchet, *J. Am. Chem. Soc.* **2010**, *132*, 7595; d) H.-C. Liao, C.-S. Tsao, T.-H. Lin, C.-M. Chuang, C.-Y. Chen, U. S. Jeng, C.-H. Su, Y.-F. Chen, W.-F. Su, *J. Am. Chem. Soc.* **2011**, *133*, 13064.

[7] a) L. Dou, C.-C. Chen, K. Yoshimura, K. Ohya, W.-H. Chang, J. Gao, Y. Liu, E. Richard, Y. Yang, *Macromolecules* **2013**, *46*, 3384; b) A. T. Yiu, P. M. Beaujuge, O. P. Lee, C. H. Woo, M. F. Toney, J. M. J. Fréchet, *J. Am. Chem. Soc.* **2011**, *134*, 2180; c) H. Zhou, L. Yang, S. C. Price, K. J. Knight, W. You, *Angew. Chem. Int. Ed.* **2010**, *49*, 7992.

[8] a) H. Hayashi, W. Nihashi, T. Umeyama, Y. Matano, S. Seki, Y. Shimizu, H. Imahori, *J. Am. Chem. Soc.* **2011**, *133*, 10736; b) F. Wessendorf, B. Grimm, D. M. Guldi, A. Hirsch, *J. Am. Chem. Soc.* **2010**, *132*, 10786; c) C.-L. Wang, W.-B. Zhang, R. M. Van Horn, Y. Tu, X. Gong, S. Z. D. Cheng, Y. Sun, M. Tong, J. Seo, B. B. Y. Hsu, A. J. Heeger, *Adv. Mater.* **2011**, *23*, 2951.

[9] a) W. Zhou, P. Shen, B. Zhao, P. Jiang, L. Deng, S. Tan, *J. Polym. Sci., Part A: Polym. Chem.* **2011**, *49*, 2685; b) X. Huang, C. Zhu, S. Zhang, W. Li, Y. Guo, X. Zhan, Y. Liu, Z. Bo, *Macromolecules* **2008**, *41*, 6895; c) S. Shi, P. Jiang, S. Chen, Y. Sun, X. Wang, K. Wang, S. Shen, X. Li, Y. Li, H. Wang, *Macromolecules* **2012**, *45*, 7806.

[10] a) A. C. Mayer, M. F. Toney, S. R. Scully, J. Rivnay, C. J. Brabec, M. Scharber, M. Koppe, M. Heeney, I. McCulloch, M. D. McGehee, *Adv. Funct. Mater.* **2009**, *19*, 1173; b) F. Huang, K.-S. Chen, H.-L. Yip, S. K. Hau, O. Acton, Y. Zhang, J. Luo, A. K. Y. Jen, *J. Am. Chem. Soc.* **2009**, *131*, 13886; c) J. Hou, L. Huo, C. He, C. Yang, Y. Li, *Macromolecules* **2005**, *39*, 594; d) M. Zhang, Y. Gu, X. Guo, F. Liu, S. Zhang, L. Huo, T. P. Russell, J. Hou, *Adv. Mater.* **2013**, *25*, 4944.

[11] J.-F. Jheng, Y.-Y. Lai, J.-S. Wu, Y.-H. Chao, C.-L. Wang, C.-S. Hsu, *Adv. Mater.* **2013**, *25*, 2445.

[12] C.-L. Wang, C.-M. Lan, S.-H. Hong, Y.-F. Wang, T.-Y. Pan, C.-W. Chang, H.-H. Kuo, M.-Y. Kuo, E. W.-G. Diau, C.-Y. Lin, *Energy Environ. Sci.* **2012**, *5*, 6933.

[13] C. V. Hoven, X.-D. Dang, R. C. Coffin, J. Peet, T.-Q. Nguyen, G. C. Bazan, *Adv. Mater.* **2010**, *22*, E63.

[14] C.-H. Hsieh, Y.-J. Cheng, P.-J. Li, C.-H. Chen, M. Dubosc, R.-M. Liang, C.-S. Hsu, *J. Am. Chem. Soc.* **2010**, *132*, 4887.

[15] C.-L. Wang, Y.-C. Chang, C.-M. Lan, C.-F. Lo, E. Wei-Guang Diau, C.-Y. Lin, *Energy Environ. Sci.* **2011**, *4*, 1788.

[16] M. Gouterman, *J. Mol. Spectrosc.* **1961**, *6*, 138.

[17] C.-F. Lo, L. Luo, E. W.-G. Diau, I. J. Chang, C.-Y. Lin, *Chem. Commun.* **2006**, 1430.

[18] Y.-C. Chang, C.-L. Wang, T.-Y. Pan, S.-H. Hong, C.-M. Lan, H.-H. Kuo, C.-F. Lo, H.-Y. Hsu, C.-Y. Lin, E. W.-G. Diau, *Chem. Commun.* **2011**, *47*, 8910.

[19] a) K. Sonogashira, Y. Tohda, N. Hagihara, *Tetrahedron Lett.* **1975**, 4467; b) S. Takahashi, Y. Kuroyama, K. Sonogashira, *Synthesis* **1980**, 627; c) R. W. Wagner, T. E. Johnson, F. Li, J. S. Lindsey, *J. Org. Chem.* **1995**, *60*, 5266.